Bulgarian Chemical Communications, Volume 54, Special Issue B2 (pp. 20-26) 2022 DOI: 10.34049/bcc.54.B2.0489

Hybrid supercapacitors with innovative binder - *ex-situ* structural and morphological studies

B. A. Karamanova[1*], P. S. Ublekov[2], L. S. Soserov[1], Ch. P. Novakov[2], I. V. Dimitrov[2], A. E. Stoyanova[1]

[1]*Institute of Electrochemistry and Energy Systems, Bulgarian Academy of Sciences, Acad. G. Bonchev Str, 10, 1113 Sofia, Bulgaria*

[2]*Institute of Polymers, Bulgarian Academy of Sciences, Acad. G. Bonchev Str, 103, 1113 Sofia, Bulgaria*

Received: January 27, 2021; Revised: July 29, 2022

In this study are presented the results from *ex-situ* physicochemical analyses of electrodes with synthesized poly(vinylidene fluoride-co-hexafluoropropylene) (P(VDF-co-HFP) used as binder in the active electrode mass of hybrid supercapacitors. The cells based on biogenic activated carbon, αβ-$Ni(OH)_2$ composite electrode, ionic liquid (1-ethyl-3-methylimidazolium tetrafluoroborate) as electrolyte and P(VDF-co-HFP) exhibit improved capacitive characteristics. The crystal structure of the electrodes is studied using X-ray diffraction analysis. The profiles of pristine $Ni(OH)_2$ electrode before and after the electrochemical tests are similar, however, decreases in peak intensity were observed in (001) and (110) directions. In contrast, the peak intensity of (100) and (101) increased, suggesting the formation of more perfect crystals. The electrode morphology is visualized by optical microscope and AFM techniques.

Keywords: hybrid supercapacitor, polymer binder, ionic liquid, electrochemical tests, *ex-situ* study

INTRODUCTION

The supercapacitors are a relatively new generation of energy-storage devices. The function of supercapacitors (SCs) is based on the reversible adsorption of electrolyte ions into electrode materials. The interaction involving the electrode and electrolyte acts as an essential function in their overall performance. Therefore, the appropriate selection of electrode materials and electrolyte determines the SC performance.

Ionic liquids (ILs) show an enormous potential in electrochemistry due to the mobility and flexibility of ions [1]. ILs are good candidates for supercapacitors, particularly those working based on the double layer charging [2, 3]. The primary task of the electrolyte is to provide charge species at the electrode/electrolyte interface instead of diffusion of specific electroactive species. The specific energy strongly depends on the potential window, which in turn depends on the electrolyte used [4, 5]. For aqueous electrolytes-based SCs the electrochemical stability potential region is about 1.0–1.2 V, while the organic electrolytes and ionic liquids (ILs)-based SCs have the potential windows 2.7–3.0 V and 3.5–4.0 V, respectively [6-10]. Therefore, the wide stable potential window of ILs guarantees high energy densities [11, 12].

Many ILs have lower conductivity, higher viscosity and therefore a narrower operating limit at lower temperatures than aqueous and non-aqueous electrolytes. However, compared to volatile aqueous and organic electrolytes, they are much safer in SC applications, especially in the case of high current densities [13, 14]. All components of this system - electrode materials and electrolyte, as well as electrolyte additives are crucial for the development of a supercapacitor with high energy and power characteristics, as well as high Faraday efficiency [15].

In spite of the potential of ILs and the growing interest in their application in these systems, there is still only a limited number of fundamental studies (mostly theoretical) focused on the electrode / electrolyte interface of supercapacitors in IL [16-19]. It is good to keep in mind that the complexity of ILs is due to the novelty of these media compared to conventional electrolytes.

In recent years, the P(VDF-co-HFP) fluorocopolymers are attracting more attention and depending on the HFP content they can act as thermoplastics, elastomers or thermoplastic elastomers [20]. P(VDF-co-HFP) copolymers exhibit high thermostability, high hydrophobicity and enhanced mechanical properties. These copolymers have already been involved in numerous applications, and more recently for various uses in the field of energy (polymer electrolyte membranes for fuel cells, Li-ion batteries, solar cells, etc.) [21].

* To whom all correspondence should be sent:
E-mail: boriana.karamanova@iees.bas.bg

The aim of the present work is to develop a hybrid supercapacitor with improved characteristics by introducing an effective polymer binder poly(vinylidene fluoride-co-hexafluoropropylene) (P(VDF-co-HFP)) in the mass of the active electrode, to perform impact conducting electrochemical tests and *ex-situ* physicochemical analyses of the electrodes.

EXPERIMENTAL

Reagents and Materials

The reagents used in the copolymerization procedure were purchased from Sigma-Aldrich. Vinylidene fluoride (VDF, ≥ 99%) and hexafluoropropylene (HFP, ≥ 99%) were used as received. Ammonium persulfate ($(NH_4)_2S_2O_8$), reagent grade, 98%) was recrystallized from distilled water prior to use. Ionic liquid (1-ethyl-3-methylimidazolium tetrafluoroborate ($EMIMBF_4$), Alfa Aesar, 98%) with acetonitrile (AN, Alfa Aesar, 99,7%) and polypropylene (PC, Alfa Aesar, 99%) additives in different concentrations was used as an electrolyte.

The active components in the electrode active mass are commercial activated carbon (YP-50F, Kurary Europe GmbH) and interstratified $\alpha\beta_{IS}$-$Ni(OH)_2$, prepared by precipitation from 0.5 M $NiSO_4$ solution with KOH at pH = 12 and temperature 70-80 °C [22].

Synthesis of poly(vinylidene fluoride-co-hexafluoropropylene) (P(VDF-co-HFP))

The copolymer synthesis was performed according to a previously described procedure [23]. Briefly, a 0.16 M aqueous solution of the radical initiator ammonium persulfate was introduced into an autoclave, degassed and purged with 2 MPa of nitrogen pressure. In the next step predetermined amounts of VDF (0.156 mol) and HFP (0.034 mol) at ratio 82/18 mol% were added and the copolymerization was carried out at 85°C for 7 h under pressure. Upon polymerization completion the autoclave was cooled down to room temperature and the emulsion was degassed in order to remove any residual unreacted VDF and/or HFP. The reaction mixture was frozen using liquid nitrogen and the copolymer was recovered through lyophilization.

Preparation of supercapacitor cells

The composite electrodes are made of activated carbon (AC) matrix with addition of $\alpha\beta_{IS}$-$Ni(OH)_2$ in content of 25%. The other electrode consists of only AC. The mass ratio between the two electrodes is 1:1, the mass loading is about 0.018 – 0.020 g. Graphite ABG 1005 EG1 (10 wt.%) and binder (10 wt. %) are added previously to the activated carbon using standardized procedure. The formed sheet electrodes are dried at 140°C for 12 h, pressed under 20 MPa and mounted in coin-type cell with Glassmat separator.

Physicochemical and electrochemical characterization

The capacitor cells were subjected to galvanostatic charge/discharge using Arbin Instrument System BU-2000 electrochemical equipment. The test program was carried out at constant current mode at different current loads and room temperature. Some cells were subjected to continuous cycling charge/discharge at a current rate of 240 mAg^{-1} up to 5000 cycles.

The specific discharge capacitance ($F\ g^{-1}$) was calculated by the equation [24]:

$$C = (I \times \Delta t)/(m \times \Delta V) \quad (1),$$

where I, Δt, m and Δ V are discharge current, discharge time, mass of active material and voltage window, respectively. On the basis of the specific discharge capacitance, the energy density (E) can be expressed as [25]:

$$E = C\ \Delta V^2 /7.2 \quad (2)$$

The surface and morphology changes in the electrodes during supercapacitor testing were analyzed by means of *ex-situ* XRD and optical microscopy techniques. The crystal structure of the samples was studied using X-ray diffraction (XRD) analysis using the Bruker D8 Advance ECO diffractometer in reflection mode with Ni-filtered Cu Kα radiation over the 2θ range of 5-60°.

Size exclusion chromatography (SEC) was conducted on a combined SEC/multi-angle laser light scattering (MALLS) system consisting of Alliance e2695 HPLC separations module (Waters Corp.), 2998 PDA (Waters Corp.), DAWN Heleos II MALLS and OptilabT-rEX DRI (Wyatt Tech.) detectors. Chromatographic separation was achieved by a set of three Novema GPC columns (PSS Polymer Standards Service GmbH) with NH-functionalized acrylate copolymer network with a nominal pore size of 30, 1000 and 1000 Å. Analyses were performed in 0.2 mol formic acid aqueous solution containing 100 mmol of NaCl as eluent at 40°C and flow rate of 1 $mL.min^{-1}$.

The morphology of the electrode surface was visualized with a Stemi 305 optical microscope.

The atomic-force microscopy (AFM) observations were performed on three separate areas from each sample. The measurement conditions were as follows: square zones with linear size 49.5

μm, equal to 2.459 nm^2 of surface area for each observation; resolution equal to 256 points per line for 256 lines; acquired imaging rate of 1 second per line, only the reference sample required much lower imaging rate of 10 s/per line; scanning in dynamic regime at 17 kHz of cantilever vibration at amplitude of 600 mV; images in *scan forward* mode per line, and *from down to up* for image recording. The AFM observations were conducted by AFM EasyScan 2 produced by Nanosurf (Switzerland), equipped by TAP190Al-G.

The contact angle measurements were performed on an Easy Drop DSA20E KRÜSS GmbH apparatus, Germany. Drops from the electrolyte with a volume of 6.3 μl were deposited on the electrode surface and the mean contact angle value was obtained by averaging at least 5 measurements for each sample.

RESULTS AND DISCUSSION

For the current investigations P(VDF-co-HFP) was synthesized *via* free radical emulsion copolymerization of vinylidene fluoride and hexafluoropropylene initiated by $(NH_4)_2S_2O_8$ [23] (Fig. 1). The molar content of HFP was kept around 18% in order to ensure the thermoplastic properties of the copolymer obtained. There was no need of using emulsifier in the polymerization process since the latex particles were stabilized by the ionic chain ends of the macromolecules exposed on the particles' surfaces. The molar-mass characteristics of the copolymer obtained were determined by size exclusion chromatography (SEC). The SEC-elugram reveals a monomodal molar mass distribution for the copolymer with Mn = 78 400 g/mol (Fig. 2). The copolymer dispersity (Mw/Mn) is 2.86 which is quite good result considering the polymerization technique used for P(VDF-co-HFP) preparation.

The synthesized poly(vinylidene fluoride-co-hexafluoropropylene) P(VDF-co-HFP) was used as a binder in the mass of the active electrode and was compared with traditionally used binders (polytetrafluoroethylene (PTFE) and polyvinylidene fluoride (PVDF)).

Figure 3 compares the galvanostatic charge/discharge curves of the supercapacitor cells with different binders and electrolyte additives.

The results of Figure 3 demonstrate the effect of electrolyte additives on one hand and the kind of binders in active electrode masse on the other on the supercapacitor properties. The comparison reveals that capacitance on the SC in electrolyte contains 22 wt.% AN and P(VDF-co-HFP) show higher values. The voltage profiles are typical for hybrid systems (Fig. 3b), as the calculated values for iR-drop in these SCs do not differ significantly (0.30 V for SC with P(VDF-co-HFP) and 0.46 V - for SC with PTFE).

The results obtained suggest that the binder acts differently on the macro- and micropores of the electrode materials and thus on their adsorption ability.

From Figure 3 can be noticed that AN-additive favors the SC characteristics. The reason for the observed effect may be the increase in the conductivity of the electrolyte. The next factor is the wetting of the electrode determined by the contact angle (listed in Table 1). In general, the electrolyte with additives wet the composite electrode better in comparison with electrolyte without additive. The wettability of electrode with P(VDF-co-HFP) copolymer as innovative binder is better (the contact angle decreases twice). This can be related to the improved performance of these SCs.

Although the contact angle in the electrolyte with PC addition is lower than that in the electrolyte with AN addition (Table 1), this SC shows worse performance. This result shows that the ongoing processes are complex and further electrochemical studies and *ex-situ* physicochemical analyses are needed for their more detailed interpretation.

The results demonstrate that the developed hybrid supercapacitor based on activated carbon and 25 wt.% αβ-Ni $(OH)_2$, polymer binder P(VDF-co-HFP) and 22 wt.% AN in the electrolyte ($EMIMBF_4$) shows highest capacitance and stable behavior. For 5000 charge/discharge cycles, this SC displays only 10% drop in discharge capacitance and over 97% efficiency (Fig. 4).

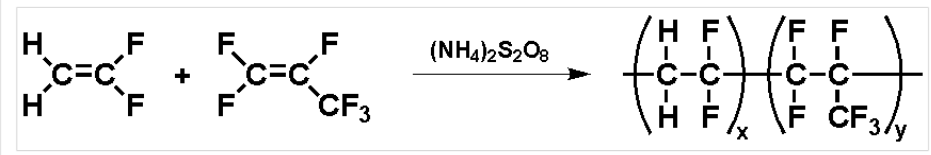

Figure 1. Synthetic route to P(VDF-co-HFP).

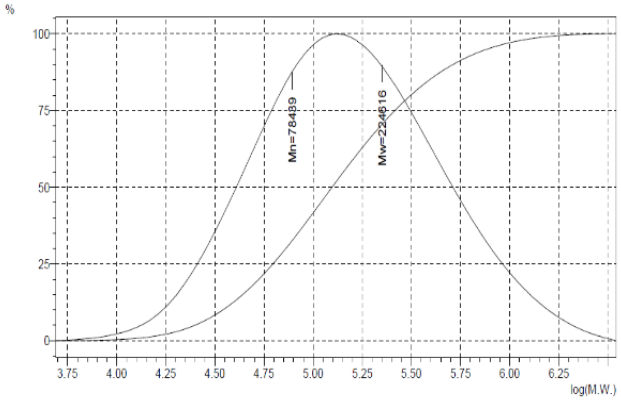

Figure 2. Size exclusion chromatogram (SEC) of P(VDF-co-HFP)

Table 1. Contact angles of composite electrode

Electrolyte	Contact angle of AC/αβ-Ni(OH)$_2$
EMIMBF$_4$(PTFE)	98.9 ° ± 2.53 °
EMIMBF$_4$+ 22 wt.% AN (PTFE)	61.9 ° ± 4.01 °
EMIMBF$_4$+ 22 wt.% AN (PVDF-co-HFP)	32.8 ° ± 2.10 °
EMIMBF$_4$+ 22 wt.% PC (PVDF-co-HFP)	19.1 ° ± 2.30 °

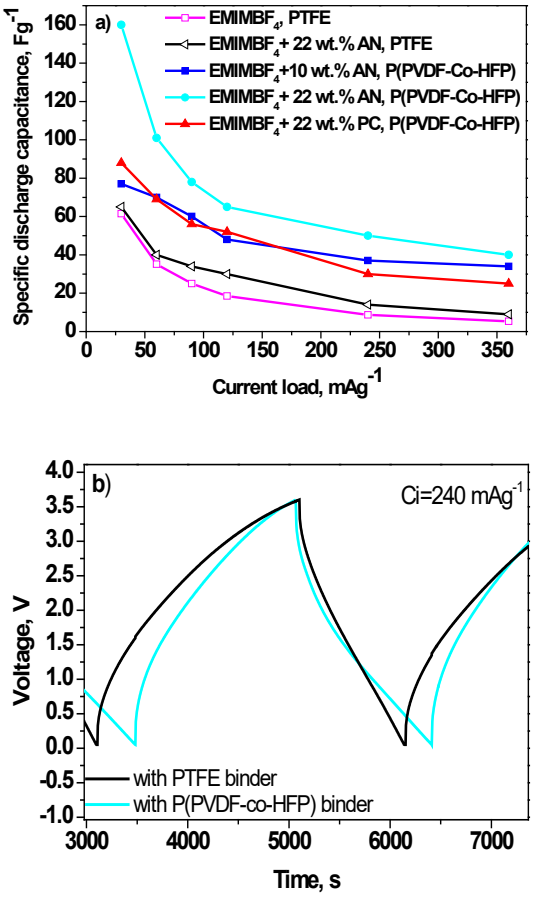

Figure 3. Discharge capacitance as a function of current load for hybrid supercapacitors (a) and galvanostatic charge/discharge profiles of SCs with different binders (b) with different binders and electrolyte additives.

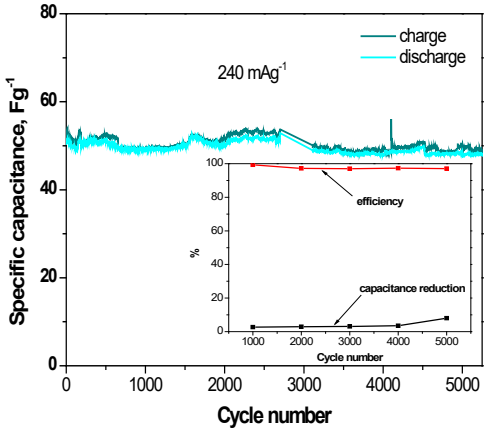

Fig. 4. Specific capacitance as a function of cycle number for SC with $EMIMBF_4$+ 22 wt.% + P(VDF-coHFP) (the inset figure shows the change in discharge capacitance and cycling efficiency during prolonged cycling)

Figure 5 compares the energy density values of supercapacitors with traditional and innovative binder. The data show a higher cell energy density with the PVDF-co-HFP binder. In interpreting the results of the electrochemical tests, it must be borne in mind that the binder has a significant effect on the pores of the activated carbon and hence on the ongoing electrochemical processes. For example, PVDF has been found to affect micro- and macropores, while PTFE predominantly attacks activated carbon macropores [26].

..

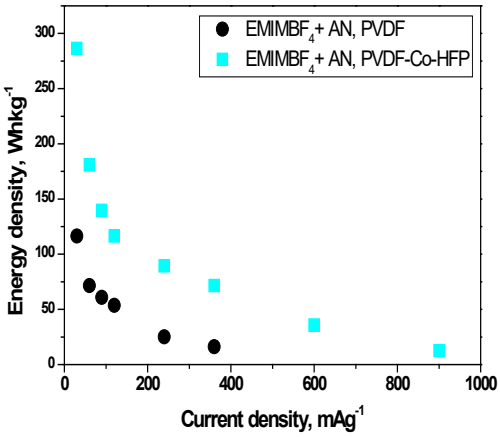

Fig. 5. Energy density as a function of current load for supercapacitors with different binders

Last but not least, the nature of the electrolyte must be taken into account. Detailed *ex-situ* physicochemical studies could serve to better clarify the positive role of the synthesized binder P(VDF-co-HFP) in the developed supercapacitor system and its further successful application in others. For this purpose, both the pristine electrodes (carbon and composite) and those after electrochemical tests were analysed.

Figure 6 compares the XRD patterns of the pristine electrodes and electrodes cycled in ionic liquid electrolyte with different binders. The XRD patterns obtained for the electrodes before and after electrochemical tests are shown in Fig. 6.

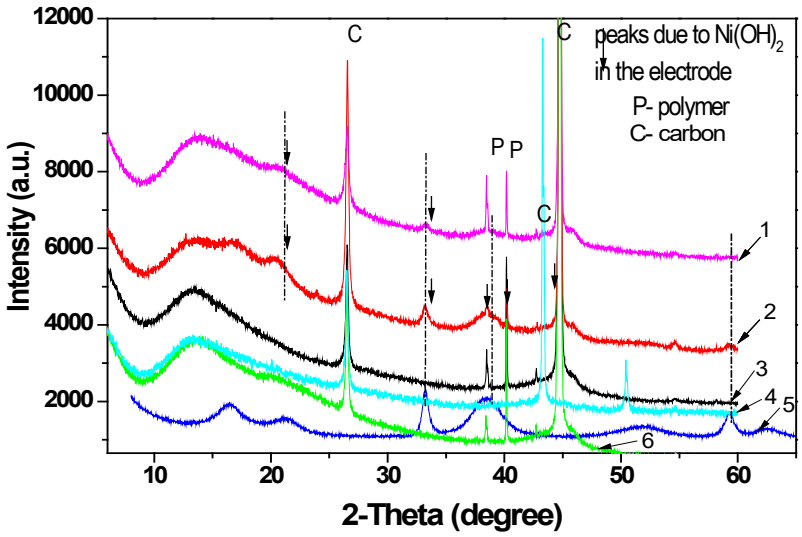

Fig. 6. XRD patterns of: 1) AC_$Ni(OH)_2$/P(VDF-co-HFP)- electrode, after electrochemical test; 2) AC_$Ni(OH)_2$/ P(VDF-co-HFP) - pristine electrode; 3) AC/ P(VDF-co-HFP) - pristine electrode; 4) AC/PVDF – pristine electrode; 5) $Ni(OH)_2$; 6) AC/ P(VDF-co-HFP) - electrode, after electrochemical test

The profile of pristine $Ni(OH)_2$ exhibited 5 prominent peaks at $2\theta = 26.6°$, 33.2°, 38.4°, 40.1° and 44.8°, corresponding to (001), (110), (100), (101), and (004) reflections of α- and β-$Ni(OH)_2$. The diffraction pattern of $Ni(OH)_2$ after electrochemical testing is similar to that of pristine α-, β-Ni(OH)2. However, decreases in peak intensity were observed in (001) and (110) directions. In contrast, the peak intensity of (100) and (101) increased, suggesting the formation of more perfect crystals of β-$Ni(OH)_2$. The α-$Ni(OH)_2$ polymorph of nickel hydroxide consists of layers of β-$Ni(OH)_2$, oriented parallel to the crystallographic ab-plane, intercalated by water molecules. The intercalated water molecules do not occupy fixed sites, but rather they have some freedom to rotate and translate? within the ab-plane. In addition to the two fundamental phases of nickel hydroxide, there are several possible types of structural disorder, including the incorporation of foreign ions, variable hydration and crystal defects including stacking faults. The effects of the structural disorder can impart very important properties. The XRD results revealed the formation of preferentially disordered β-$Ni(OH)_2$ after electrochemical testing leading to better electrochemical activity [27].

The changes in the morphology of the electrode surface after the electrochemical examination are shown in Fig. 7 (visualized with an optical microscope).

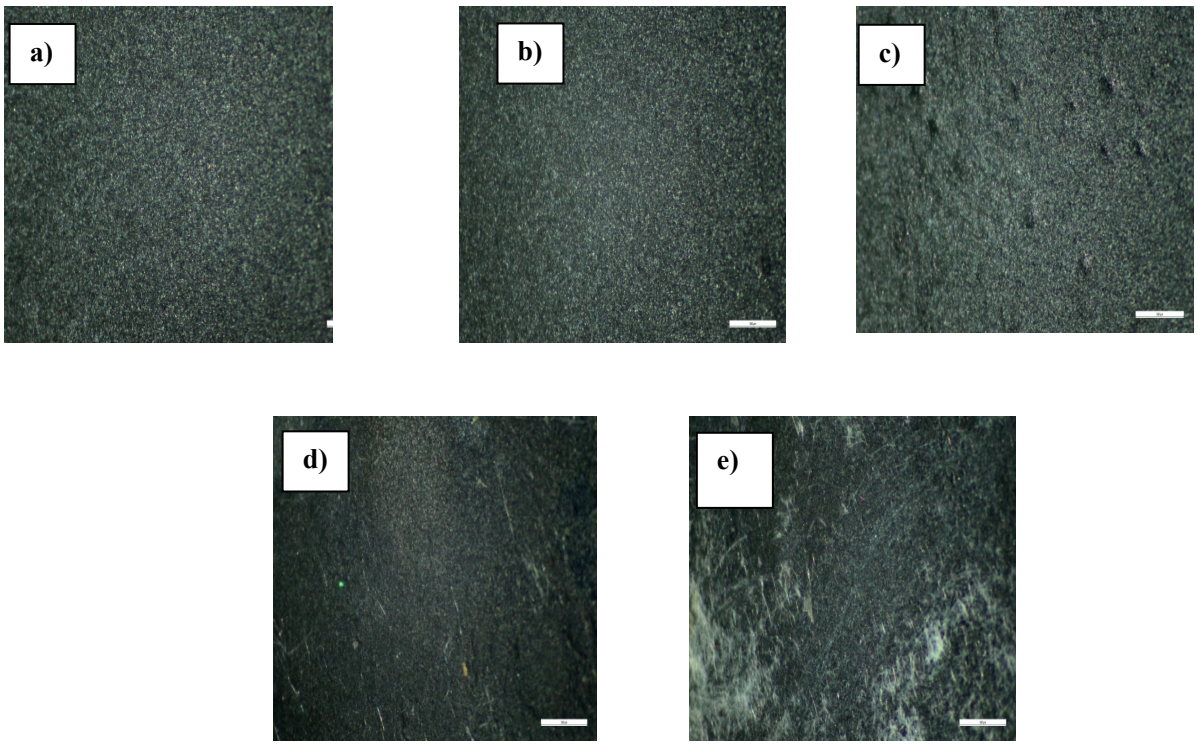

Fig. 7. Optical image of pristine and electrodes after electrochemical tests: a) C/PVDF -pristine, b) C/ P(VDF-co-HFP)- pristine, c) C_$Ni(OH)_2$/ P(VDF-co-HFP) - pristine, d) C/ P(VDF-co-HFP)- after electrochemical test, e) C_$Ni(OH)_2$/ P(VDF-co-HFP)- after electrochemical test.

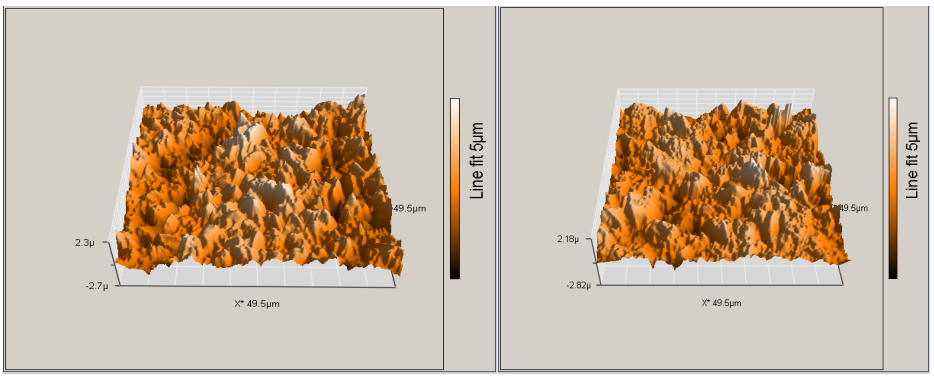

Fig. 8. 3D AFM image of the pristine electrodes: C/PVDF (left) and C/ P(VDF-co-HFP) (right)

The images show that the surface of the P(VDF-co-HFP)-modified carbon electrode is relatively smoothest, especially after electrochemical tests.

To quantify the electrode roughness AFM measurements were performed. Fig. 8 illustrates 3D AFM images of pristine carbon electrodes with classical and innovative co-polymer binders.

The results of the AFM topological observations were quantitatively evaluated. As a measure of the surface roughness are used the average value Sa, expressed by the average sum of the module of distances of all points from the measured surface, in direction, perpendicular to the conditional plane. The comparison of AFM images shows that the roughness of electrode with polymer binder is lower, Sa drops from 503.8 nm for electrode with traditional binder to 439.13 nm for the electrode with P(VDF-co-HFP). Electrode surface smoothing reactions provide more homogeneous contact with the electrolyte, resulting in higher capacitance. *Ex-situ* AFM observations of electrochemically tested carbon electrodes, as well as of composite electrodes in hybrid supercapacitor cells are forthcoming.

CONCLUSION

A new hybrid supercapacitor is demonstrated based on introduction of a synthesized specific functional co-polymer as binder in the active mass in electrode matrix. Its presence favors the wettability of the electrode while smoothing its surface thus ensuring easier penetration of IL into the pores of the carbon material. *Ex-situ* physicochemical analyzes show that the P(VDF-co-HFP) does not undergo a change during the course of electrochemical tests in contrast to the AC/Ni$(OH)_2$ – part of crystals of α-Ni$(OH)_2$ polymorph morphology transforms into disordered β-Ni$(OH)_2$ thus playing a significant role in improving the electrochemical characteristics of the studied systems.

Acknowledgements*: The financial support of the Bulgarian Ministry of Education and Science under the National Research Programme E+: Low Carbon Energy for the Transport and Households, grant agreement D01-214/2018 and the National Roadmap for Research Infrastructures, grant agreement DO1-160/28.08.2018: Energy Storage and Hydrogen Energetics (ESHER) is gratefully acknowledged.*

REFERENCES

1. A. Eftekhari, Y. Liu, P. Chen, *J Power Sources,* **334**, 221 (2016).
2. R. Jamil, D. Silvester, *Curr. Opin. Electrochem.,* **35**, 101046 (2022).
3. S. Pan, M. Yao, J. Zhang, B. Li, C. Xing, X. Song, P. Su, H. Zhang, *Front. Chem***., 8**, 261 (2020).
4. A. Eftekhar, *Energy Storage Mater.*, **9**, 47 (2017).
5. C. Zhong, Y. Deng, W. Hu, J. Qiao, L. Zhangd, J. Zhang, *Chem. Soc. Rev*., **44**, 7484 (2015).
6. L. Siinor, C. Siimenson, K. Lust, E. Lust, *Electrochem. Commun.*, **35**, 5 (2013).
7. S. Yamazaki, T. Ito, M. Yamagata, M. Ishikawa, *Electrochim. Acta,* **86**, 294 (2012).
8. C. Siimenson, M. Lembinen, O. Oll, L. Lall, M. Tarkanovskaja, V. Ivaništšev, L. Siinor, T. Thomberg, K. Lust, E. Lust, *J. Electrochem. Soc.*, **163**, H723 (2016).
9. N. Ma, N. Phattharasupakun, J. Wutthiprom, C. Tanggarnjanavalukul, P. Wuanprakhon, P. Kidkhunthod, M. Sawangphruk*, Electrochim. Acta*, **271**, 110 (2018).
10. J. Zhao, G. Gorbatovski, O. Oll, T. Thomberg, E. Lust, *Electrochim. Acta,* **31**, 82 (2019).
11. K. Aken, M. Beidaghi, Y. Gogotsi, *Angew. Chem. Int. Ed*., **54**, 4806 (2015).
12. M. Watanabe, M. Thomas, S. Zhang, K. Ueno, T. Yasuda, K. Dokko, *Chem. Rev.,* **117, 7190** (2017).
13. L. Wei, G. Yushin, *J. Power Sources,* **196**, 4072 (2011).
14. B. Scrosati, J. Hassoun, Y.-K. Sun, *Energy Environ. Sci*., **4,** 3287 (2011).
15. F. Malchik, N. Shpigel, M.D. Levi, T. Mathis, A. Mor, Y. Gogotsi, D. Aurbach, *J. Mater. Chem. A.,* **7,** 19761 (2019).
16. C. Merlet, C. Péan, B. Rotenberg, P. Madden, P. Simon, M. Salanne, *J. Phys. Chem. Lett.,* **4,** 264 (2013).
17. C. Merlet, B. Rotenberg, P. Madden, P. Taberna, P. Simon, Y. Gogotsi, M. Salanne, *Nat. Mater*., **11,** 306 (2012).
18. C. Merlet, C. Pean, B. Rotenberg, P.A. Madden, B. Daffos, P. Taberna, P. Simon, M. Salanne, *Nat. Commun.*, **4**, 2701 (2013).
19. C. Péan, C. Merlet, B. Rotenberg, P.A. Madden, P. Taberna, B. Daffos, M. Salanne, P. Simon, *ACS Nano*, **8**, 1576 (2014).
20. T. Ahmed, J. DeSimone, J. G. Roberts, *Macromolecules,* **40,** 9322 (2007).
21. B. Ameduri, *Chem. Rev.*, **109,** 6632 (2009).
22. L. Soserov, A. Stoyanova, T. Boyadzhieva, V. Koleva, M. Kalapsazova, *Electrochim. Acta*, **283,** 1063 (2018).
23. M. Apostolo, V. Arcella, G. Storti, M. Morbidelli, *Macromolecules* **32**, 989 (1999).
24. T. Wang, S. Zhang, X. Yan, M. Lyu, L. Wang, J. Bell, *ACS Appl. Mater. Interfaces,* **9,** 15510 (2017).
25. J. Huang, P. Xu, D. Cao, X. Zhou, G. Wang*, J. Power Sources*, **246**, 371 (2014).
26. L. Soserov, A. Stoyanova, R. Stoyanova, *Bulg. Chem. Commun*., **49,** 15 (2017).
27. D. Hall, D. Lockwood, C. Bock, B. MacDougal, *Proc. R. Soc. A,* **471**, 20140792 (2015).